Extreme-Ultraviolet Vortices from a Free-Electron Laser

Primož Rebernik Ribič,[1,*] Benedikt Rösner,[2] David Gauthier,[1] Enrico Allaria,[1] Florian Döring,[2] Laura Foglia,[1]
Luca Giannessi,[1,4] Nicola Mahne,[1] Michele Manfredda,[1] Claudio Masciovecchio,[1] Riccardo Mincigrucci,[1]
Najmeh Mirian,[1] Emiliano Principi,[1] Eléonore Roussel,[1] Alberto Simoncig,[1] Simone Spampinati,[1]
Christian David,[2] and Giovanni De Ninno[1,3]

[1]*Elettra-Sincrotrone Trieste, Strada Statale 14-km 163,5, 34149 Basovizza, Trieste, Italy*
[2]*Paul Scherrer Institut, 5232 Villigen-PSI, Switzerland*
[3]*Laboratory of Quantum Optics, University of Nova Gorica, 5001 Nova Gorica, Slovenia*
[4]*ENEA, C.R. Frascati, Via E. Fermi 45, 00044 Frascati (Rome), Italy*
(Received 20 June 2017; published 28 August 2017; corrected 19 July 2018)

Extreme-ultraviolet vortices may be exploited to steer the magnetic properties of nanoparticles, increase the resolution in microscopy, and gain insight into local symmetry and chirality of a material; they might even be used to increase the bandwidth in long-distance space communications. However, in contrast to the generation of vortex beams in the infrared and visible spectral regions, production of intense, extreme-ultraviolet and x-ray optical vortices still remains a challenge. Here, we present an *in-situ* and an *ex-situ* technique for generating intense, femtosecond, coherent optical vortices at a free-electron laser in the extreme ultraviolet. The first method takes advantage of nonlinear harmonic generation in a helical undulator, producing vortex beams at the second harmonic without the need for additional optical elements, while the latter one relies on the use of a spiral zone plate to generate a focused, micron-size optical vortex with a peak intensity approaching 10^{14} W/cm^2, paving the way to nonlinear optical experiments with vortex beams at short wavelengths.

I. INTRODUCTION

Optical vortices are helically phased light beams with a field dependence of $\exp(il\phi)$, where l is the topological charge and ϕ the azimuthal coordinate in the plane perpendicular to the beam propagation [1]. Such beams carry an orbital angular momentum (OAM) of $l\hbar$ per photon. The interaction between matter and extreme-ultraviolet (XUV) optical vortices is predicted to trigger new phenomena. Among these are violation of dipolar selection rules during photoionization [2], generation of charge current loops in fullerenes with an associated orbital magnetic moment [3], and the production of Skyrmionic defects [4], which show promise for applications in nanoscale magnetic memory devices. Recent theoretical and experimental advances in the field of generation and application of XUV vortex beams [5] have led to proposals for new material characterization techniques such as OAM dichroism [6] for studying technologically important materials (e.g., cuprates, manganites, and ruthenates) and stimulated emission depletion

(STED)-like microscopy [7] for enhancing the imaging resolution without the need to use fluorophores. Potential applications may even include super-resolution laser machining and long-distance space communications [8].

Most of the above-mentioned proposals require an ultra-short, high-intensity XUV or x-ray source capable of producing vortex beams. As opposed to optical vortex generation in the visible and infrared (IR) spectral regions, where such beams have been successfully used in a wide array of applications ranging from particle manipulation [9,10] and detection of spinning objects [11,12] to optical communications [13] and super-resolution imaging [14], generation of intense XUV or x-ray vortices still remains a challenging task and is undergoing extensive research.

Recently, two groups reported on the production of XUV beams with tunable topological charge using high-harmonic generation in a wave-mixing setup [8,15]. In Ref. [16], significant experimental progress was made towards plasma-based vortex generation [17,18], which shows promise for producing intense harmonics of the driving laser with adjustable OAM. However, the current performance of such tabletop systems in terms of the intensity of the generated XUV light is orders of magnitude lower compared to the new generation of accelerator-based sources such as free-electron lasers (FELs) [19], and may not be sufficient to perform some of the proposed
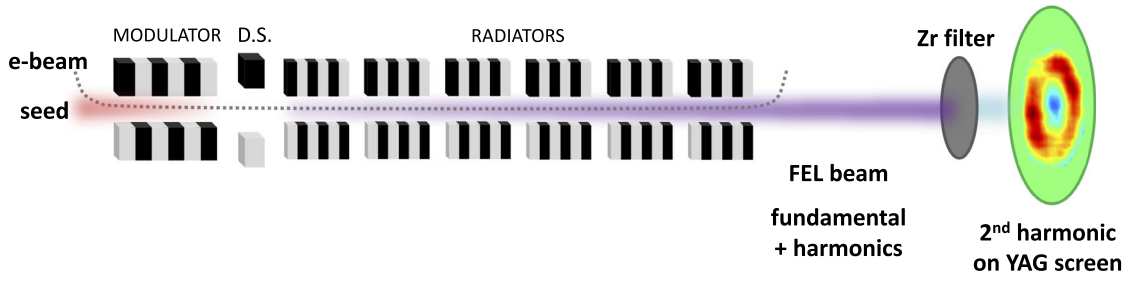
[*]primoz.rebernik@elettra.eu

FIG. 1.   Generation of coherent optical vortices through nonlinear harmonic generation at a FEL (not to scale). A transversely Gaussian seed density modulates the e-beam using a combination of an undulator (modulator) and a dispersive section (D.S.) so that it emits coherent XUV light in the radiator. The interaction between FEL radiation at the fundamental wavelength and the e-beam induces bunching at the second harmonic, which is amplified along the radiator chain, leading to emission of intense, coherent optical vortices in the XUV spectral range. A Zr filter is placed at the FEL output to suppress the fundamental Gaussian mode, transmitting only the optical vortex.

experiments. Therefore, several schemes are being studied for producing optical vortices at a FEL.

In a FEL, light is generated by relativistic electrons wiggling inside a periodic magnetic field of an undulator [20]. The interaction between the emitted light and the electrons leads to exponential amplification of the emission, producing intense (gigawatt peak power) pulses with laserlike properties. In special FEL operation modes, XUV or x-ray vortices may be generated, e.g., by bunching the electrons into a helical pattern either using a seed laser with a proper transverse phase structure [21,22] or through the interaction of the electron beam (e-beam) with a laser having a Gaussian transverse profile in a helical undulator [23]. The first scheme has the potential to produce vortex beams at high harmonics of the seed laser but has yet to be demonstrated in practice, while the latter one works only at the fundamental wavelength (i.e., the setup acts as a mode converter) and therefore requires a coherent seed laser in the XUV or x-ray wavelength range. XUV vortices can also be produced by placing a diffractive optical element, such as a phase mask or a computer-generated hologram, directly into the XUV beam path. This method was successfully used to generate vortex beams at synchrotrons [24,25]; however, for FELs, the optical elements have to be properly designed to withstand the extremely high photon flux, and up to now, there are no reports of XUV vortex generation at a FEL using such direct approaches.

Here, we demonstrate two methods for generating intense XUV beams carrying OAM. In the first one, we take advantage of the vortex nature of harmonics emitted in a helical undulator [26,27]; however, unlike the previous experiment [28], where XUV vortices were produced by incoherent undulator emission, we exploit high-harmonic [29] and nonlinear harmonic generation [30–33] to obtain intense, femtosecond, coherent XUV vortices from a chain of six undulators at the FERMI FEL [34]. The method can be easily implemented at existing FEL facilities. The second technique relies on the use of a spiral zone plate (SZP) [35], which is placed

directly into the FEL beam path. The setup produces a focused, micron-sized, high-intensity optical vortex without requiring extensive modifications of the FEL beamline.

II. COHERENT OPTICAL VORTICES FROM NONLINEAR HARMONIC GENERATION

Recent theoretical studies demonstrated that vortex beams emitted by free electrons may be more ubiquitous than previously thought. It was shown that harmonic components of radiation produced by a relativistic electron moving on a circular or spiral trajectory, such as the one in a helical undulator, carry a total (spin and orbital) angular momentum of $n\hbar$ per photon, where n is the harmonic number [27]. In the paraxial regime, this translates into an OAM content corresponding to $l = n - 1$; see Ref. [26]. Although it has been known for a while that harmonics emitted by a helical undulator show a characteristic donut-like distribution with zero on-axis intensity [33,36,37], the helical phase of such radiation has only recently been addressed in more detail [26,27]. These theoretical predictions were first confirmed in a synchrotron experiment using a helical undulator to produce optical vortices in the XUV spectral range [28]. However, in a synchrotron, the emission from individual electrons, which are randomly distributed within the e-beam, adds up incoherently, resulting in a relatively low intensity and poor temporal coherence of the emitted light. Both the temporal coherence and intensity can be strongly enhanced by density modulating the e-beam at the emission wavelength with a seed laser. This scheme was used in Ref. [38] to generate coherent optical vortices in the IR from a single undulator.

Here, we extend the approach to the XUV spectral range by exploiting the principles of high-harmonic [29] and nonlinear harmonic generation [30–33]. The experiment was performed at the FERMI FEL [34]. An ultraviolet (250-nm) seed laser was used to energy modulate the e-beam in the first undulator (modulator), as shown in Fig. 1. The e-beam was then sent through a dispersive

section (a four-dipole-magnet chicane), where the energy modulation was transformed into a current-density modulation (bunching) with Fourier components spanning many harmonics of the seed laser frequency. Such a bunched e-beam entered the helical radiator tuned to a fundamental wavelength of 31.2 nm (i.e., the eighth harmonic of the seed), producing coherent light in the XUV. The FEL was operated in the high-gain regime, close to the saturation point [39,40]. Under these conditions, the interaction between the radiation at the fundamental FEL wavelength and the e-beam induces bunching at the second harmonic (15.6 nm); see, e.g., Ref. [41]. Contrary to the experiment in Ref. [38] where optical vortices were produced by coherent harmonic generation using only a single undulator, the bunching at the second harmonic (already present after the dispersive section) was maintained, and the resulting coherent emission was amplified along the whole undulator chain, giving intensities at the second harmonic on the order of 10^{-3} of the fundamental FEL emission [42].

For the scheme to work, the e-beam trajectory has to be centered through all the radiator sections so that emission from each undulator interferes constructively in the transverse plane. Any deviations from the ideal e-beam trajectory result in the distortion of the OAM mode. The electron trajectory was carefully aligned using the fundamental emission (Gaussian mode) from each radiator. First, the seed laser path was aligned with the e-beam trajectory in the modulator. The downstream e-beam trajectory was then adjusted by tuning each of the radiator sections one by one, while maintaining the direction of the resulting emission. The transverse intensity distribution was collected 50 m downstream from the last radiator by inserting a YAG screen, which was imaged by a CCD camera. The result is shown in the top panel of Fig. 2 and resembles a laserlike Gaussian pattern with an additional ringlike intensity distribution. Such an intensity pattern is the result of interference from six 2.42-m-long radiator sections, whose emission is aligned along the same optical axis, separated by 1.1-m-long drift spaces to accommodate the e-beam focusing optics; see Fig. 1. The intensity distribution is in very good agreement with a simple model, where a Gaussian-mode emission was assumed for each of the undulators (see Fig. 2, bottom panel). Because of different wave-front curvatures [43] at the YAG screen, the interference produces an additional ringlike pattern with a radius of around 7 mm from the beam axis. To reproduce the experimental pattern, we fixed the electric field strengths by measuring the emission intensities from each of the undulators (most of the intensity was coming from the last four radiator sections). The only free parameter was the root mean square (rms) radiation size, which was determined to be ~55 μm, in relatively good agreement with the theoretical rms e-beam size, assuming a normalized (slice) emittance of 1 mm mrad at an e-beam energy of 1.1 GeV, and an average beta function of 8 m. The
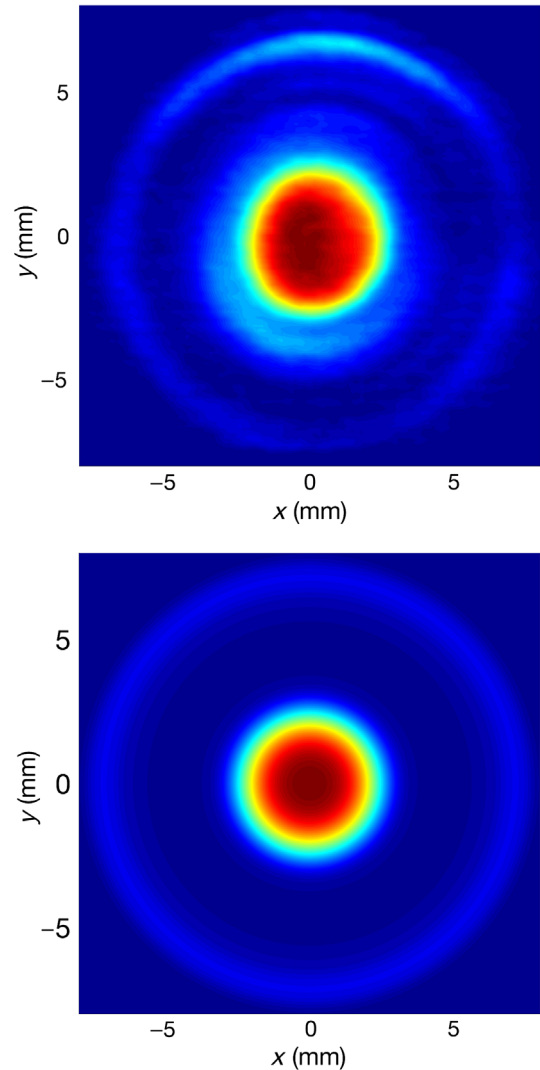

FIG. 2. A typical single-shot interference pattern of the FEL emission from a chain of six undulators. Top panel: Experiment. Bottom panel: Calculation (obtained assuming emission only at the fundamental wavelength).

asymmetries in the experimental interference pattern indicate small deviations from the ideal e-beam trajectory and/or asymmetries in the e-beam transverse distribution.

The spot in Fig. 2 is a superposition of the field emitted by the undulators at the fundamental frequency and its higher-order harmonics [44]. A 100-nm Zr filter allowed us to suppress (by a factor of 10^{-6}) the fundamental Gaussian mode and observe only the emission at the second harmonic. The result in the left panel of Fig. 3 shows a typical hollow intensity distribution, characteristic of an optical vortex. Because of the small e-beam size, the divergence angle of light from each of the undulators was relatively high, resulting in a multi-ring-like interference pattern in the far field. Furthermore, because of enhanced sensitivity to wave-front distortions of the radiation at the second harmonic, the intensity pattern was not
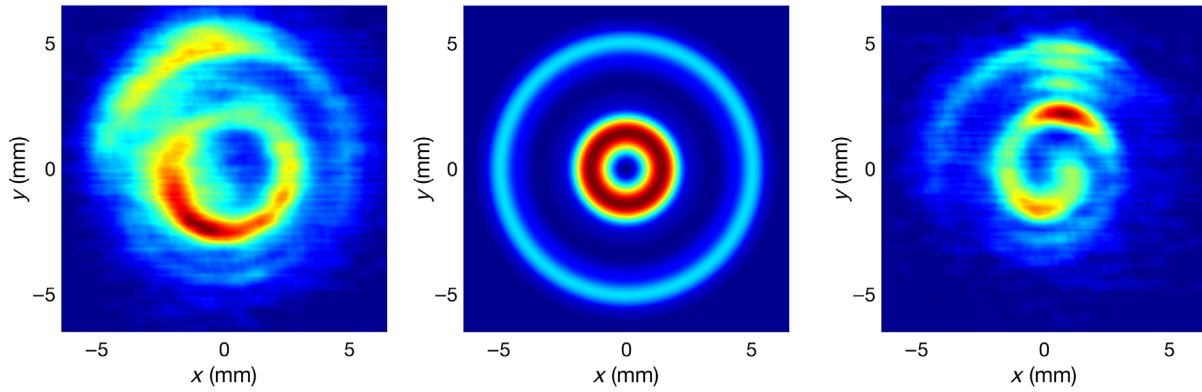
FIG. 3.   Left panel: A typical single-shot image of an optical vortex generated at 15.6 nm. The multiple-ring pattern comes from the interference of the emission from six undulators. Middle panel: Calculation. Right panel: A single-spiral pattern obtained by interference of the optical vortex with a Gaussian mode (in a single-shot measurement), confirming the $l = 1$ charge of the vortex beam.

perfectly symmetric for the two observed rings. In the middle panel in Fig. 3, we calculated the intensity distribution assuming a Laguerre-Gaussian $l = 1$ [1] mode emitted from each of the undulators. Despite its simplicity, the model qualitatively reproduces the measured intensity distribution, although the size of the inner ring is underestimated.

To confirm the vortex nature of the emitted light, we performed an interference experiment by tuning the first undulator to a resonant wavelength corresponding to the second harmonic of the following undulators. The interference between the Gaussian mode produced by the first radiator section and the OAM-carrying light from the rest of the undulators gave a single spiral structure [28], a clear proof that the vortex beam carried a topological charge of $l = n - 1 = 1$, as shown in the right panel of Fig. 3.

In an effort to obtain an optical vortex that can be described with a single Laguerre-Gaussian transverse mode, we increased the e-beam size to ~ 85 μm by decreasing the strength of the focusing quadrupoles between the radiator sections. This resulted in a smaller emission angle from each undulator and decreased interference features, giving a

single donut-shaped emission pattern, characteristic of a single Laguerre-Gaussian mode, as shown in Fig. 4. The interference with the Gaussian emission mode from the first undulator again revealed an $l = 1$ charged beam. From the measurements, we estimated an intensity ratio between the second harmonic and the fundamental emission of $\sim 3 \times 10^{-3}$, in good agreement with theory [42].

III. COHERENT OPTICAL VORTICES FROM A SPIRAL ZONE PLATE

A high-intensity optical vortex can also be obtained by putting a SZP directly into the optical path of the fundamental (transversely Gaussian) FEL beam. The SZP simultaneously imprints a helical phase onto the FEL beam and focuses it, just like an ordinary Fresnel zone plate, generating a focused optical vortex [45]. This possibility was demonstrated with synchrotron radiation [35,46], yet the high photon flux at a FEL imposes serious limitations for the design of such zone plates, as many common materials cannot withstand even the unfocused FEL beam intensity [47]. An excellent
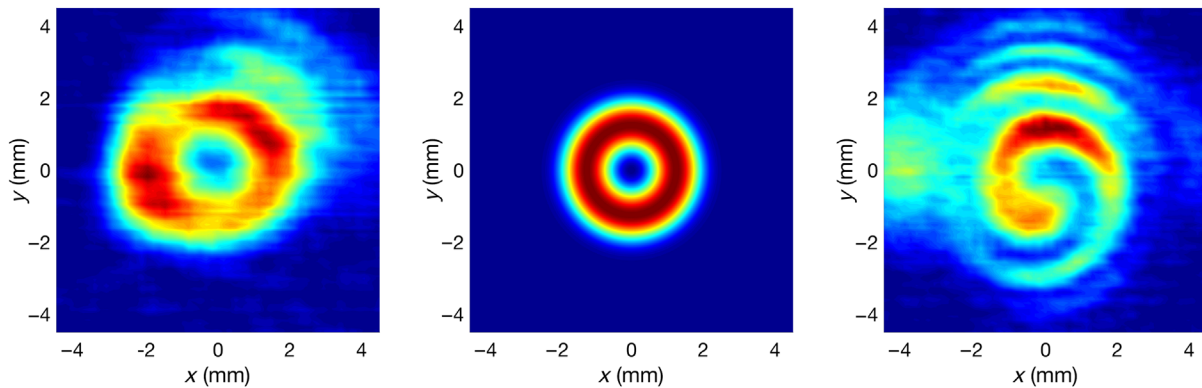

FIG. 4.   Left panel: A typical single-shot image of the donut-shaped intensity pattern obtained by increasing the e-beam size. Middle panel: Calculation. Right panel: A single-spiral pattern obtained by interference of the optical vortex with a Gaussian mode (in a single-shot measurement), confirming the $l = 1$ charge of the vortex beam.
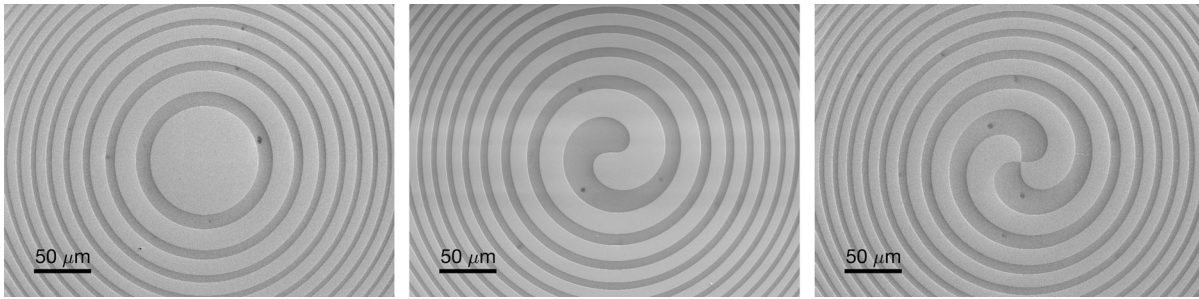
FIG. 5.   SEM images of ZPs with charges of $l = 0$ (left panel), $l = 1$ (middle panel), and $l = 2$ (right panel).

material for the fabrication of radiation-hard diffractive optical elements in the XUV regime is silicon [48], with a damage threshold above 4 J/cm^2, several orders of magnitude higher than the energy density used in our experiment.

The SZPs used in the experiment were etched into ultra-flat, 340-nm-thick silicon membranes. For this purpose, the silicon membrane was coated with a chromium layer and a polymer resist, which was subsequently exposed with the zone plate pattern using e-beam lithography. After development, the pattern was transferred into the chromium layer by reactive ion etching (RIE), which was then used as a hard mask in a subsequent RIE step to etch the zone plates 200–230 nm deep into the silicon membrane.

Figure 5 shows scanning electron microscope (SEM) images of an ordinary Fresnel zone plate (ZP) and SZPs with topological charges of 1 and 2. The ZPs were designed for a wavelength of 26 nm and had a focal length of 120 mm. The ZP diameter was 1.90 mm, with an outermost zone width of 1.64 μm. The lateral dimensions of opaque and transparent zones were adjusted to a ratio of 60:40. This geometry almost completely suppresses the zeroth diffraction order (the directly transmitted FEL beam) that carries no OAM without the use of a central beam stop.

The experimental layout is sketched in Fig. 6. A motorized setup (not shown) was installed into an experimental chamber ~100 m downstream of the last radiator section to align the ZPs with respect to the FEL beam. The setup included a 2-mm upstream pinhole to limit the FEL beam size (~6 mm) and a set of downstream pinholes

placed into the focal plane to filter out the negative and higher diffraction orders, allowing for exclusive detection of the first diffraction order.

Because of micrometer spot sizes, the detection of the phase was performed in the far field with a Hartmann wave-front sensor (WFS) [49] mounted 80 cm downstream of the ZP focus. The results are shown in the left and middle columns of Fig. 7. To characterize the focal spot, an imprint technique was used [50]. With this method, the transverse intensity distribution was obtained by analyzing the holes made by the FEL beam in a poly-methylmethacrylate (PMMA) layer by ablation. Using the Beer-Lambert law and taking into account the mean free path of XUV light in PMMA, the depth of the imprints reflects the intensity on a logarithmic scale; see right column in Fig. 7.

The standard ZP (see first row in Fig. 7) produces a Gaussian-like beam in the far field with an almost flat phase profile, after removing the quadratic curvature introduced by focusing; the residual phase contrast (0.25 rad rms) is due to the aberrations of the mirrors that were used to steer the FEL beam into the experimental chamber, aberrations in the FEL beam itself, and the WFS detection noise. The reconstructed focus from the PMMA imprints shows the typical diffraction pattern of the zone plate, which is described very well with the first-order Bessel function, with a Rayleigh spot size of 2.0 μm, in exact agreement with theory. Assuming 17% efficiency for the ZP and a typical energy per pulse of 10 μJ for a 50-fs pulse duration used during the experiment, a power density on the order of 10^{14} W/cm^2 is estimated in the focus. The zone
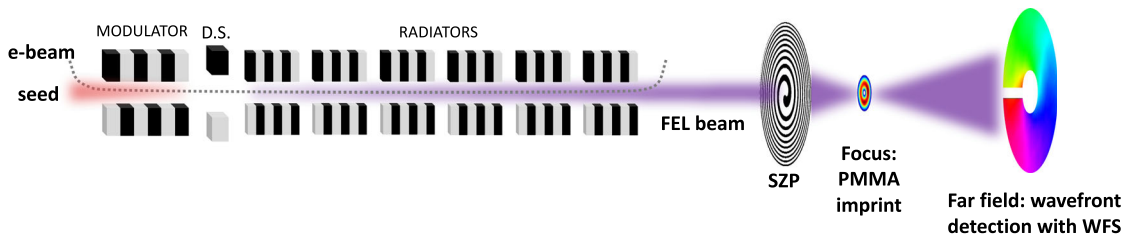

FIG. 6.   Generation of intense, coherent XUV vortices at the fundamental FEL wavelength with a SZP. The fundamental, transversely Gaussian FEL beam was sent onto the SZP, producing a micron-size optical vortex in the focal plane, which was detected using the PMMA imprint method; see text for details. The spiral phase of the vortex was measured in the far field (80 cm from the focal plane) with a WFS.
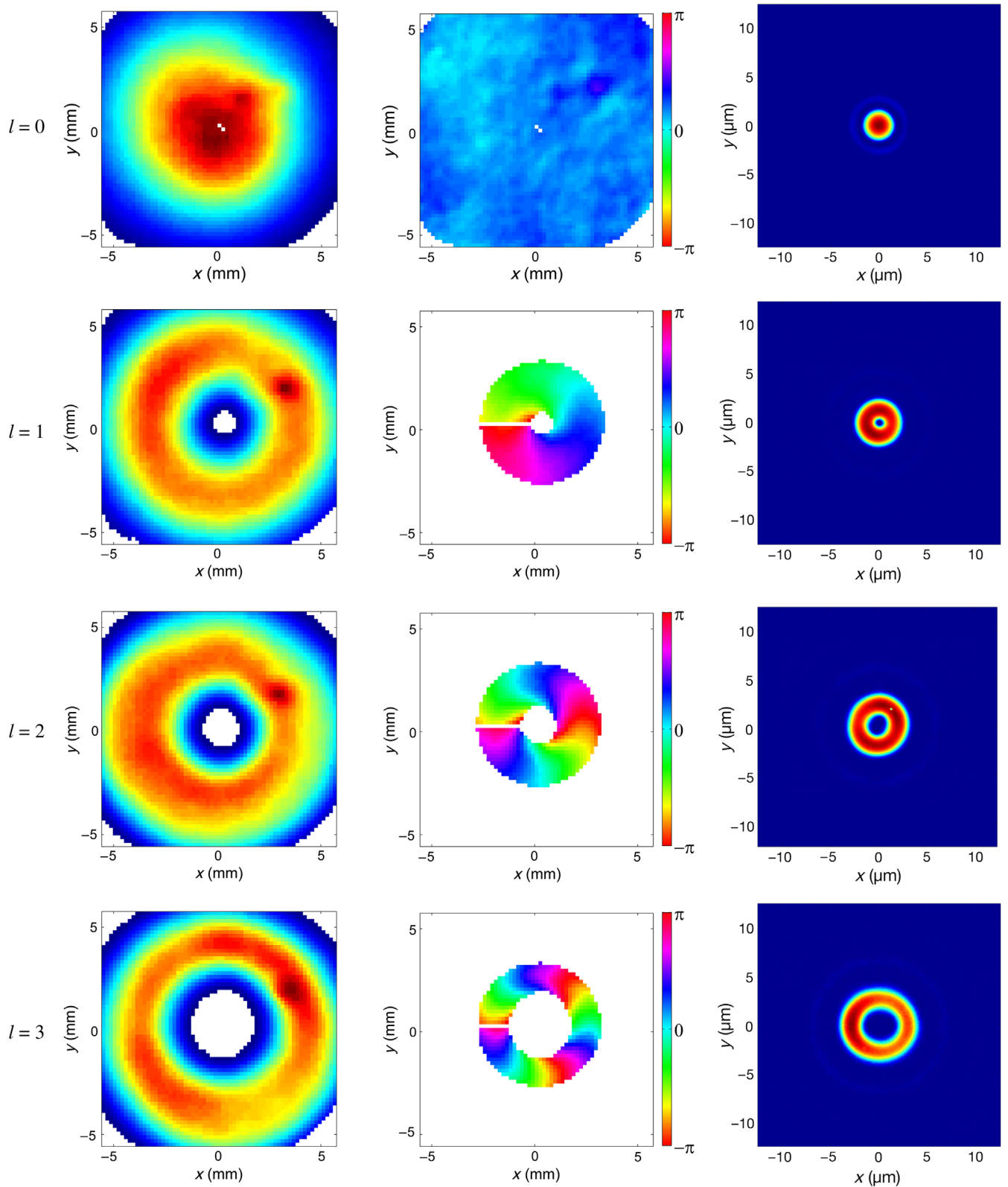
FIG. 7.   Measured far-field intensity (left column) and phase (middle column), and the intensity distribution in the focal plane (right column) for ZPs with charges from 0 (top row) to 3 (bottom row). Because of the relatively long distance from the focus (800 mm), the phase gradients were below the detection threshold of the WFS far from the beam axis. We therefore had to limit the reconstruction of the phase to a circle with a radius of around 3 mm from the singularity point, as shown for $l = 1$, 2, and 3. All measurements were done in single-shot mode.

widths, and thus the spot size of the ZP in focus, can be reduced by a factor of 50–100, which, in combination with an energy per pulse of 100 μJ, routinely achieved at FERMI, would increase the power density by at least 4 orders of magnitude.

The second, third, and fourth rows in Fig. 7 show the measured intensities and phases for $l = 1$, 2, and 3. A characteristic donut-shaped intensity pattern is found in the far field with a spiral phase gradient whose integration around the singularity gives approximately $2\pi l$, confirming the vortex nature of the beams produced by the SZPs. The small discrepancies, e.g., on the order of 10% for $l = 2$, between the theoretical and experimental values for the integrated phase are attributed to a relatively low sampling of the wave front [15]. The focus again shows a character-istic donut-shaped intensity distribution with an accompa-nying Airy-like ring, as for the $l = 0$ case. As expected, the diameter of the donut-shaped rings in the left and right columns in Fig. 7 increases with topological charge. As a control experiment, we also tested SZPs with opposite helicity, which produced optical vortices with a reversed helical phase pattern (not shown).

IV. DISCUSSION

We presented two methods to generate intense, femto-second, coherent optical vortices in the XUV spectral region. In the first scheme, we took advantage of nonlinear harmonic generation in a FEL to produce coherent $l = 1$ vortex beams at the second harmonic from a chain of six helical undulators. The setup does not require placing additional optical elements into the FEL beam path (except the filter for the fundamental) and can also be used to generate optical vortices with higher topological charges according to the formula $l = n - 1$, by exploiting emission at higher harmonics. The sign of the topological charge can simply be controlled by controlling the helicity of the fundamental emission [28,51]. In the second scheme, a SZP was placed directly into the optical path of the fundamental (transversely Gaussian) FEL beam to generate a high-intensity, focused optical vortex. A set of different SZPs allowed us to produce $l = \pm 1$, 2, 3 charged vortices. For $l = 1$, a peak intensity in the focal plane of 10^{14} W/cm^2 can be easily obtained by using an energy of 100 μJ per FEL pulse, without damaging the ZPs. This value can be increased up to 10^{17} W/cm^2 or more by using SZPs with smaller zone widths. In the case where a high-intensity optical vortex is not required, the SZP setup can also be used at an HHG-based source after isolating the desired harmonic from the rest of the spectrum. In principle, both methods described above can be used for the generation of vortex beams at even shorter wavelengths (soft and hard x-ray spectral regions) [52].

To our knowledge, this is the first demonstration of the generation of intense XUV optical vortices at a FEL. The methods developed here will allow carrying out some of the recently proposed experiments involving vortex beams in different areas of fundamental and applied physics ranging from optics to magnetic switching and from material characterization to super-resolution laser machining.

[1] L. Allen, M. W. Beijersbergen, R. J. C. Spreeuw, and J. P. Woerdman, *Orbital Angular Momentum of Light and the Transformation of Laguerre-Gaussian Laser Modes*, Phys. Rev. A **45**, 8185 (1992).

[2] A. Picón, A. Benseny, J. Mompart, J. R. Vázquez de Aldana, L. Plaja, G. F. Calvo, and L. Roso, *Transferring Orbital and Spin Angular Momenta of Light to Atoms*, New J. Phys. **12**, 083053 (2010).

[3] J. Wätzel, Y. Pavlyukh, A. Schäffer, and J. Berakdar, *Optical Vortex Driven Charge Current Loop and Optomagnetism in Fullerenes*, Carbon **99**, 439 (2016).

[4] H. Fujita and M. Sato, *Ultrafast Generation of Skyrmionic Defects with Vortex Beams: Printing Laser Profiles on Magnets*, Phys. Rev. B **95**, 054421 (2017).

[5] C. Hernández-García, J. Vieira, T. J. Mendonça, L. Rego, J. San Román, L. Plaja, P. R. Ribič, D. Gauthier, and A. Picón, *Generation and Applications of Extreme-Ultraviolet Vortices*, Photonics **4**, 28 (2017).

[6] M. van Veenendaal and I. McNulty, *Prediction of Strong Dichroism Induced by X Rays Carrying Orbital Momentum*, Phys. Rev. Lett. **98**, 157401 (2007).

[7] G. Gariepy, J. Leach, K. T. Kim, T. J. Hammond, E. Frumker, R. W. Boyd, and P. B. Corkum, *Creating High-Harmonic Beams with Controlled Orbital Angular Momentum*, Phys. Rev. Lett. **113**, 153901 (2014).

[8] F. Kong *et al.*, *Controlling the Orbital Angular Momentum of High Harmonic Vortices*, Nat. Commun. **8**, 14970 (2017).

[9] H. He, M. E. J. Friese, N. R. Heckenberg, and H. Rubinsztein-Dunlop, *Direct Observation of Transfer of Angular Momentum to Absorptive Particles from a Laser Beam with a Phase Singularity*, Phys. Rev. Lett. **75**, 826 (1995).

[10] T. Kuga, Y. Torii, N. Shiokawa, T. Hirano, Y. Shimizu, and H. Sasada, *Novel Optical Trap of Atoms with a Doughnut Beam,* Phys. Rev. Lett. **78,** 4713 (1997).

[11] M. P. J. Lavery, F. C. Speirits, S. M. Barnett, and M. J. Padgett, *Detection of a Spinning Object Using Light's Orbital Angular Momentum,* Science **341,** 537 (2013).

[12] D. B. Phillips, M. P. Lee, F. C. Speirits, S. M. Barnett, S. H. Simpson, M. P. J. Lavery, M. J. Padgett, and G. M. Gibson, *Rotational Doppler Velocimetry to Probe the Angular Velocity of Spinning Microparticles,* Phys. Rev. A **90,** 011801 (2014).

[13] J. Wang *et al. Terabit Free-Space Data Transmission Employing Orbital Angular Momentum Multiplexing,* Nat. Photonics **6,** 488 (2012).

[14] A. Jesacher, S. Fürhapter, S. Bernet, and M. Ritsch-Marte, *Shadow Effects in Spiral Phase Contrast Microscopy,* Phys. Rev. Lett. **94,** 233902 (2005).

[15] D. Gauthier *et al. Tunable Orbital Angular Momentum in High-Harmonic Generation,* Nat. Commun. **8,** 14971 (2017).

[16] A. Denoeud, L. Chopineau, A. Leblanc, and F. Quéré, *Interaction of Ultraintense Laser Vortices with Plasma Mirrors,* Phys. Rev. Lett. **118,** 033902 (2017).

[17] X. Zhang, B. Shen, Y. Shi, X. Wang, L. Zhang, W. Wang, J. Xu, L. Yi, and Z. Xu, *Generation of Intense High-Order Vortex Harmonics,* Phys. Rev. Lett. **114,** 173901 (2015).

[18] J. Vieira, R. M. G. M. Trines, E. P. Alves, R. A. Fonseca, J. T. Mendonća, R. Bingham, P. Norreys, and L. O. Silva, *High Orbital Angular Momentum Harmonic Generation,* Phys. Rev. Lett. **117,** 265001 (2016).

[19] P. R. Ribič and G. Margaritondo, *Status and Prospects of X-Ray Free-Electron Lasers (X-FELs): A Simple Presentation,* J. Phys. D **45,** 213001 (2012).

[20] G. Margaritondo and P. R. Ribič, *A Simplified Description of X-Ray Free-Electron Lasers,* J. Synchrotron Radiat. **18,** 101 (2011).

[21] E. Hemsing and A. Marinelli, *Echo-Enabled X-Ray Vortex Generation,* Phys. Rev. Lett. **109,** 224801 (2012).

[22] P. R. Ribič, D. Gauthier, and G. De Ninno, *Generation of Coherent Extreme-Ultraviolet Radiation Carrying Orbital Angular Momentum,* Phys. Rev. Lett. **112,** 203602 (2014).

[23] E. Hemsing, A. Knyazik, M. Dunning, D. Xiang, A. Marinelli, C. Hast, and J. B. Rosenzweig, *Coherent Optical Vortices from Relativistic Electron Beams,* Nat. Phys. **9,** 549 (2013).

[24] A. G. Peele, P. J. McMahon, D. Paterson, C. Q. Tran, A. P. Mancuso, K. A. Nugent, J. P. Hayes, E. Harvey, B. Lai, and I. McNulty *Observation of an X-Ray Vortex,* Opt. Lett. **27,** 1752 (2002).

[25] B. Terhalle, A. Langner, B. Päivänranta, V. A. Guzenko, C. David, and Y. Ekinci, *Generation of Extreme Ultraviolet Vortex Beams Using Computer Generated Holograms,* Opt. Lett. **36,** 4143 (2011).

[26] S. Sasaki and I. McNulty, *Proposal for Generating Brilliant X-Ray Beams Carrying Orbital Angular Momentum,* Phys. Rev. Lett. **100,** 124801 (2008).

[27] M. Katoh, M. Fujimoto, H. Kawaguchi, K. Tsuchiya, K. Ohmi, T. Kaneyasu, Y. Taira, M. Hosaka, A. Mochihashi, and Y. Takashima *Angular Momentum of Twisted Radiation from an Electron in Spiral Motion,* Phys. Rev. Lett. **118,** 094801 (2017).

[28] J. Bahrdt, K. Holldack, P. Kuske, R. Müller, M. Scheer, and P. Schmid, *First Observation of Photons Carrying Orbital Angular Momentum in Undulator Radiation,* Phys. Rev. Lett. **111,** 034801 (2013).

[29] L. H. Yu, *Generation of Intense UV Radiation by Subharmonically Seeded Single-Pass Free-Electron Lasers,* Phys. Rev. A **44,** 5178 (1991).

[30] J. B. Murphy, C. Pellegrini, and R. Bonifacio, *Collective Instability of a Free Electron Laser Including Space Charge and Harmonics,* Opt. Commun. **53,** 197 (1985).

[31] R. Bonifacio, L. De Salvo, and P. Pierini, *Large Harmonic Bunching in a High-Gain Free-Electron Laser,* Nucl. Instrum. Methods Phys. Res., Sect. A **293,** 627 (1990).

[32] H. P. Freund, S. G. Biedron, and S. V. Milton, *Nonlinear Harmonic Generation in Free-Electron Lasers,* IEEE J. Quantum Electron. **36,** 275 (2000).

[33] G. Geloni, E. Saldin, E. Schneidmiller, and M. Yurkov, *Theory of Nonlinear Harmonic Generation in Free-Electron Lasers with Helical Wigglers,* Nucl. Instrum. Methods Phys. Res., Sect. A **581,** 856 (2007).

[34] E. Allaria *et al. Highly Coherent and Stable Pulses from the FERMI Seeded Free-Electron Laser in the Extreme Ultraviolet,* Nat. Photonics **6,** 699 (2012).

[35] A. Sakdinawat and Y. Liu, *Soft-X-Ray Microscopy Using Spiral Zone Plates,* Opt. Lett. **32,** 2635 (2007).

[36] E. Allaria, F. Curbis, M. Coreno, M. Danailov, B. Diviacco, C. Spezzani, M. Trovó, and G. De Ninno, *Experimental Characterization of Nonlinear Harmonic Generation in Planar and Helical Undulators,* Phys. Rev. Lett. **100,** 174801 (2008).

[37] R. Barbini, F. Ciocci, G. Dattoli, and L. Giannessi, *Spectral Properties of the Undulator Magnets Radiation: Analytical and Numerical Treatment,* Riv. Nuovo Cimento **13,** 1 (1990).

[38] E. Hemsing, M. Dunning, C. Hast, T. Raubenheimer, and D. Xiang, *First Characterization of Coherent Optical Vortices from Harmonic Undulator Radiation,* Phys. Rev. Lett. **113,** 134803 (2014).

[39] R. Bonifacio, C. Pellegrini, and L. M. Narducci, *Collective Instabilities and High-Gain Regime in a Free Electron Laser,* Opt. Commun. **50,** 373 (1984).

[40] E. L. Saldin, E. A. Schneidmiller, and M. V. Yurkov, *Statistical and Coherence Properties of Radiation from X-Ray Free-Electron Lasers,* New J. Phys. **12,** 035010 (2010).

[41] G. Dattoli, L. Giannessi, and A. Torre, *Unified View of Free-Electron Laser Dynamics and of Higher-Harmonics Electron Bunching,* J. Opt. Soc. Am. B **10,** 2136 (1993).

[42] D. Ratner *et al. Second and Third Harmonic Measurements at the Linac Coherent Light Source,* Phys. Rev. ST Accel. Beams **14,** 060701 (2011).

[43] E. Ferrari, *Experimental characterization of FEL polarization control with cross polarized undulators,* in *Proceedings of the 36th International Free-Electron Laser Conference* (2014), http://accelconf.web.cern.ch/AccelConf/FEL2014/papers/tha02.pdf.

[44] The intensities of higher-order harmonics are much weaker compared to the fundamental one. Therefore, only emission at the fundamental mode was used in the analytical model.

[45] N. R. Heckenberg, R. McDuff, C. P. Smith, and A. G. White, *Generation of Optical Phase Singularities by Computer-Generated Holograms*, Opt. Lett. **17**, 221 (1992).

[46] J. Vila-Comamala, A. Sakdinawat, and M. Guizar-Sicairos, *Characterization of X-Ray Phase Vortices by Ptychographic Coherent Diffractive Imaging*, Opt. Lett. **39**, 5281 (2014).

[47] C. David *et al. Nanofocusing of Hard X-Ray Free Electron Laser Pulses Using Diamond Based Fresnel Zone Plates*, Sci. Rep. **1**, 57 (2011).

[48] J. Vila-Comamala, K. Jefimovs, J. Raabe, B. Kaulich, and C. David, *Silicon Fresnel Zone Plates for High Heat Load X-Ray Microscopy*, Microelectron. Eng. **85**, 1241 (2008).

[49] P. Mercère *et al. Hartmann Wave-Front Measurement at 13.4 nm with λEUV/120 Accuracy*, Opt. Lett. **28**, 1534 (2003).

[50] J. Chalupský *et al. Spot Size Characterization of Focused Non-Gaussian X-Ray Laser Beams*, Opt. Express **18**, 27836 (2010).

[51] M. Katoh *et al. Helical Phase Structure of Radiation from an Electron in Circular Motion*, Sci. Rep. **7**, 6130 (2017).

[52] E. Allaria *et al. Two-Stage Seeded Soft-X-Ray Free-Electron Laser*, Nat. Photonics **7**, 913 (2013).